Processing of Polypropylene–Clay Nanocomposites: Single-Screw Extrusion with In-Line Supercritical Carbon Dioxide Feed versus Twin-Screw Extrusion

Mark A. Treece, James P. Oberhauser

Department of Chemical Engineering, University of Virginia, Charlottesville, Virginia 22904

Received 22 June 2006; accepted 10 August 2006
DOI 10.1002/app.25226
Published online in Wiley InterScience (www.interscience.wiley.com).

ABSTRACT: This work investigates two different melt-blending strategies for preparing compatibilized polypropylene-clay nanocomposites, specifically: (1) conventional twin-screw extrusion, and (2) single-screw extrusion capable of direct supercritical carbon dioxide (scCO$_2$) feed to the extruder barrel. Proportional amounts (3 : 1) of maleic anhydride functionalized polypropylene compatibilizer and organically modified montmorillonite clay at clay loadings of 1, 3, and 5 wt % are melt-blended with a polypropylene homopolymer using the two approaches. The basal spacing, degree of exfoliation, and dispersion of organoclay is assessed using X-ray diffraction, transmission electron microscopy, and rheology. In terms of the latter, both steady shear and small-amplitude oscillatory shear provide information about the apparent yield stress and solid-like terminal behavior respectively. Finally, nanoindentation is performed to determine the room temperature modulus of each melt-blended nanocomposite. The results reveal unequivocally that the high shear of the twin-screw process is vastly superior to the single-screw with in-line scCO$_2$ addition in generating well-exfoliated, percolated polypropylene-clay nanocomposites. It is likely that increased contact time between clay and scCO$_2$ is necessary for scCO$_2$ to positively affect exfoliation. © 2006 Wiley Periodicals, Inc. J Appl Polym Sci 103: 884–892, 2007

Key words: polypropylene; organoclay; nanocomposites; microstructure; supercritical carbon dioxide

INTRODUCTION

Polymer–clay nanocomposites (PCNs) have recently attracted significant attention due to marked property enhancements at mass loadings substantially less than conventional fillers. For instance, increased tensile strength and modulus along with improved barrier resistance, flame retardation, and heat distortion characteristics have been reported for many common polymers upon addition of only a few weight percent clay.[1–4] These remarkable property enhancements make nanocomposites superior candidates as materials for food packaging, electronics, and automotive industries. One of the most commonly utilized nanofillers is derived from montmorillonite (MMT). MMT has a structure consisting of several stacked layers with a layer thickness of 0.98 nm and lateral dimension of 400–1000 nm. These silicate layers are separated by a charged intergallery that preserves a fixed spacing between layers. The sum of the intergallery dimension and the individual silicate layer thickness is defined as the basal spacing (d_{001} spacing) and measurable by X-ray diffraction (XRD).[3] Because the natural clay is hydrophilic, surface modification of the clay is required to render it organophilic and thereby miscible with many common polymers. Surface modification is typically performed by ion-exchange reactions using primary, secondary, tertiary, and quaternary alkylammonium surfactants.[4] As a result, the basal spacing is expanded, allowing for improved intercalation of polymer into the intergallery and better physical interaction between the clay and polymer. For highly nonpolar polymers (e.g., polypropylene, polyethylene), intercalation is thermodynamically unfavorable; consequently, it is necessary to incorporate a compatibilizer into the nanocomposite blend. A compatibilizer consists of polymer functionalized by side- or end-groups, such as maleic anhydride, that have more favorable thermodynamic interactions with the clay surface yet retain miscibility with the polymer.[5]

Optimal dispersion of clay in the polymer matrix is necessary to maximize the interfacial contact between the polymer and clay and, thus, macroscopic property enhancement. The dispersion of clay in a PCN is characterized as either: (1) *agglomerated*, where the layered silicates aggregate and display limited physical or chemical interaction with the polymer; (2) *intercalated*, where polymer diffuses into the clay intergallery, fur-

Correspondence to: J. P. Oberhauser (oberhauser@virginia.edu).

Contract grant sponsor: National Science Foundation (NSF); contract grant number: CTS-0134275.

ther swelling the spacing between layers without completely destroying the coherence of those layers; or (3) *exfoliated*, where individual clay platelets are separated and dispersed within the polymer matrix. Because the high aspect ratio of the individually dispersed platelets generates the largest surface area to volume ratio, exfoliation leads to better phase homogeneity and the greatest improvements in thermal and mechanical properties.[6,7]

The ability to promote organoclay exfoliation is strongly tied to the preparation and blending of PCNs. *In situ* polymerization and solution blending methods of producing nanocomposites have been successfully employed for a number of polymers. Other efforts involve *in situ* polymerization of polymers such as polystyrene (PS) and poly(methyl methacrylate) (PMMA) via bulk, solution, suspension, and emulsion polymerization.[8,9] However, because these methods require large quantities of expensive, environmentally unfriendly solvents, melt-blending with high shear remains the most practical method of preparing PCNs.[4] Recently, a great deal of attention has been given to synthesizing nanocomposite systems with the aid of supercritical CO_2 ($scCO_2$) to expand the clay intergallery and promote polymer intercalation.[10] $scCO_2$ offers a number of practical advantages over other solvents. It is relatively inexpensive and environmentally friendly (i.e., nontoxic, nonflammable) compared with organic solvents,[11] and it possesses unique properties, including high diffusivity, low viscosity, near-zero surface tension, and the ability to solubilize many common polymers.[12] Recent efforts have utilized $scCO_2$ to pretreat clay and as a solvent directly injected to an extruder during melt-blending. For example, Manke et al. devised a process in which the clay is first saturated with $scCO_2$ in a partitioned vessel and then rapidly depressurized to forcibly break apart clay platelets.[13,14] The pretreated clay was then compounded via conventional melt-blending, resulting in a substantially more exfoliated PCN relative to samples not subjected to $scCO_2$ pretreatment. Direct injection of $scCO_2$ into a molten nanocomposite during melt-blending is also promising, since the same rapid depressurization employed in conjunction with shear may further improve clay exfoliation. Garcia-Leiner et al. recently reported data for a polyethylene (PE)-MMT nanocomposite processed in a modified single screw extruder equipped with $scCO_2$ injection near the feed hopper.[15] Their results show a 40–100% increase in basal spacing and suggest that $scCO_2$ processing plays a significant role in facilitating melt intercalation and clay dispersion.

This study compares compatibilized polypropylene (PP)-MMT nanocomposites with 1, 3, and 5 wt % clay loadings prepared using two melt-blending techniques. The first is a novel single-screw extrusion (SSE) system capable of direct $scCO_2$ feed to the extruder barrel during processing. The system is designed to inject $scCO_2$ into the molten polymer–clay mixture to facilitate exfoliation and dispersion of clay platelets. This system is contrasted with a conventional twin-screw extrusion (TSE) process to assess whether $scCO_2$ addition could replace the need for the high shear processing. The exfoliation and dispersion are probed with XRD, transmission electron microscopy (TEM), and mechanical rheology. Nanoindentation is also performed to assess the mechanical properties of the nanocomposites.

EXPERIMENTAL

Materials

Polypropylene (PP, Dow Chemical Co., grade H700-12, MFI = 12 g/10 min at 230°C and 2.16 kg load, M_w = 229 kg/mol, M_w/M_n = 3.98) was used as the matrix polymer. Southern Clay Products provided Cloisite® 15A (C15A, 125 meq/100 g, d_{001} = 3.15 nm), a natural MMT clay modified with a quaternary ammonium salt. Polybond® 3200 (pp-*g*-MA, Crompton Corp., MFI = 110 g/10 min at 190°C and 2.16 kg load), a 1 wt % maleic anhydride functionalized polypropylene, was used as the compatibilzer.

Melt-blending was conducted in two ways. First, single-screw extrusion (SSE) (Killion Extruder, L/D = 52, D = 25.4 mm) with direct addition of $scCO_2$ was employed with barrel temperatures set at 190–210°C and a screw speed of 15 rpm. The $scCO_2$ was injected to the extruder approximately 2/3 of the distance down the barrel length using a MuCell® supercritical fluid system (Trexel Inc.) to ensure complete melting of the polymer before the introduction of $scCO_2$. The density of $scCO_2$ leaving the chiller was 843.2 kg/m^3, and the flow rate was set to 5% of the extrusion rate to match the maximum absorption capacity of CO_2 in polypropylene.[16] Material was cycled through the extruder twice, the second pass without $scCO_2$ addition to ensure adequate mixing of the nanocomposite and remove the foam generated by the first pass.

Conventional TSE was conducted with a Leistritz Micro 27 extruder (L/D = 52, D = 27 mm) was operated with barrel temperatures ranging from 200–210°C and corotating screws rotating at 200 rpm. PP was dry mixed with the compatibilizer and metered at 5 lb/h to the screws. Clay was added through a side stuffer positioned at the halfway length of the screw (26D) and set at a metering rate appropriate to the desired clay loading. Both techniques were used to prepare samples with a fixed 3 : 1 ratio of PB3200 compatibilizer to clay, and clay loadings of 1, 3, and 5 wt %. Additionally, a control material consisting of 10 wt % pp-*g*-MA and 90% PP was also prepared using the SSE-$scCO_2$ process.

X-ray diffraction

Samples studied with XRD were compression molded at 190°C to a thickness of ≈1.5 mm. XRD experiments were conducted using a Scintag XDS 2000 diffractometer with a Cu Kα radiation source (λ = 1.540562 Å). Data were collected with a step size of 0.02° and a scan rate of 0.5°/min. The results presented are the average of four scans. The location of scattering peaks was used to measure the clay basal spacing (d_{001} peak) as influenced by the two blending procedures.

Transmission electron micrsocopy

Transmission electron microscopy (TEM) using a JEOL 2000FX microscope operated at 200 kV was used to image the final clay morphology produced by each mixing strategy. Bright-field images were taken at ×60,000 on microtomed sections (70–90 nm thick) of each sample. TEM images complement XRD, providing qualitative information on the degree of clay exfoliation and dispersion.

Rheology

Since it is well-known that rheology is sensitive to the microstructure of filled polymer melts, steady shear and small-amplitude oscillatory shear (SAOS) rheological experiments were conducted to assess the dispersion of clay in each nanocomposite sample.[17–23] All experiments were performed with a TA Instruments AR 2000 rheometer using a 25-mm parallel plate geometry and environmental test chamber (ETC). A nitrogen purge of 10 L/min was continuously supplied to the ETC to inhibit oxidative degradation of the polypropylene during experimentation. Compression molded samples (190°C) were initially melted at 210°C for 10 min in the rheometer, after which the upper plate was lowered to a gap distance of 1 mm for rheological testing.

Steady shear rate sweeps were performed from low to high shear rates (0.01–1.0 s^{-1}) at 180°C on all nanocomposites. Prior work has shown that some PCNs behave as constant shear-thinning materials.[20,24,25] That is, they exhibit shear thinning at low shear rates where the matrix polymer would be characterized by its zero-shear viscosity. This divergence of viscosity at low shear rates is consistent with the presence of a finite apparent yield stress and is interpreted as a strong indicator of clay networking above the mechanical percolation threshold.[18,24] The continuous shear thinning is a hydrodynamic effect arising from the increased orientation of anisotropic clay domains in the flow direction (or alternatively, with surface normal perpendicular to the flow direction). Thus, for highly filled, well-exfoliated samples, flow-induced orientation of clay domains and divergent shear thinning behavior are expected. On the other hand, samples with low clay loadings and poor exfoliation are expected to exhibit the liquid-like rheology characteristic of the polymer melt with only a modest increase in the zero-shear viscosity resulting from the inclusion of a dilute concentration of solid particles. In this fashion, steady shear flow experiments offer a means of qualitatively assessing the degree of exfoliation and dispersion of clay.

Oscillatory shear is particularly sensitive to the development of a solid-like clay network in the PCN. First, oscillatory stress sweeps from 1 to 10,000 Pa were performed at 180°C and a constant frequency of 1 rad/s to identify the boundary of the linear viscoelastic regime and determine the critical strain (or stress) at which the rheological response becomes nonlinear. Several authors have reported that the critical strain is sensitive to the clay loading and microstructure, with the critical strain shifting to lower values with increasing solid volume fraction.[22,25,26] SAOS frequency sweeps were also conducted, as numerous studies of filled polymeric liquids have revealed the presence of a solid-like plateau for the storage modulus (G') in the terminal regime. Such behavior has been attributed to the formation of a mesoscale clay network at loadings above the percolation threshold.[18,20,23,27] The strain value was chosen to be 1% to ensure a linear response, and consecutive frequency sweeps were carried out at temperatures of 210, 180, and 150°C. Time–temperature superposition (TTS) was subsequently performed with a reference temperature of 180°C.

Nanoindentation

Nanoindentation experiments were performed with a MTS NANO Indenter® XP (MTS Systems) using a standard continuous stiffness module to measure the modulus of each nanocomposite at room temperature. For a given indentation event, the Berkovich pyramid diamond indenter was brought in contact with the surface, followed by penetration of the surface to a depth of 5 μm at a constant strain rate of 0.1 s^{-1}. The indenter was held for 10 s at that depth and then withdrawn at the same rate. A minimum of 15 indentations were conducted for each sample, and the distance between any two indentations was at least 100 μm. The reported modulus values were calculated by averaging the results of all indentations. Because the averaging was performed only on measurements taken well below the surface (2–5 μm), the result is indicative of the bulk modulus of the material.

RESULTS AND DISCUSSION

X-ray diffraction

XRD scans for each nanocomposite and dry C15A clay are presented in Figure 1, and the resultant basal spac-

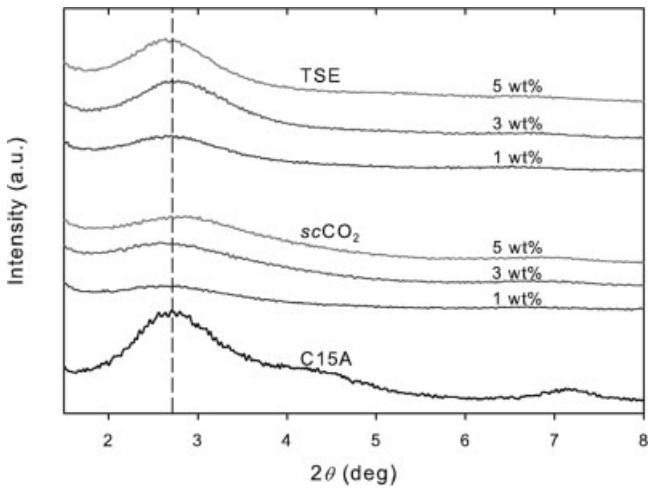

Figure 1 XRD scans for 1, 3, and 5 wt % scCO$_2$ and TSE nanocomposites compared with those for dry C15A clay.

ings inferred from Bragg's law are summarized in Table I. First, we observe that the basal spacing measured for the dry C15A clay is slightly larger (32.6 Å) than that quoted by the manufacturer (31.5 Å); however, the difference is unimportant, since shifts in nanocomposite basal spacing relative to the dry clay is most germane to this discussion. Examining the data, it is apparent that the 1 wt % scCO$_2$, 3 wt % scCO$_2$, and all three TSE samples show statistically insignificant changes in basal spacing relative to the dry C15A clay as a result of melt-blending. Only the 5 wt % scCO$_2$ sample is unique, as its basal spacing decreases modestly compared with the dry clay and other nanocomposites. It should be noted that the amount of scCO$_2$ introduced to the extruder was constant, independent of clay loading. As a result, the ratio of scCO$_2$ to clay decreased with increasing clay loading, which may be a factor in the scCO$_2$ results. In general, however, XRD reveals no significant structural changes in these nanocomposite samples at the length scale of the intergallery spacing. Moreover, XRD cannot provide information about the number of platelets per tactoid, making it is a poor standalone technique for assessing the degree of exfoliation.[7,28] Because the organically modified C15A already has a large intergallery dimension (relative to the 1.17 Å of natural MMT), additional swelling of the intergallery without exfoliation may be difficult to achieve. The larger length scales relevant to mechanical percolation and mesoscale clay structure must be probed by other means. Nevertheless, these data emphasize the important conclusion that neither melt-blending procedure alters the average intergallery spacing to a meaningful degree.

Finally, it is interesting to note that the magnitude of the peak intensity for the scCO$_2$ samples is smaller than that of the TSE samples. While one might ascribe this difference to improved exfoliation of the scCO$_2$ samples, results presented in the subsequent sections contradict such a hypothesis. Instead, we believe that the difference in intensity is related to sample preparation. As in other published work, XRD samples were compression molded to a desired thickness, which invariably induces a modest radial flow. While fixing the sample thickness eliminates it as a factor in affecting the peak intensity, the radial flow may flow-align anisotropic organoclay domains. The propensity of organoclay domains to be oriented by flow should depend upon their aspect ratio, where those with highest aspect ratio (i.e., fewest silicate layers or most exfoliated) are most readily aligned. The peak intensity in XRD is related to the number of diffraction events that occur as the X-ray beam passes through the sample. For a sample in which the distribution of organoclay orientation states is skewed in favor of a particular direction, the number of diffraction events associated with a particular angle may increase. Consequently, the larger peak intensity for the TSE samples indicates a larger number of diffraction events and suggests that it may contain a greater number of higher aspect ratio organoclay domains than the scCO$_2$ materials. While this hypothesis cannot be justified on the basis of XRD data alone and must be supported by TEM and rheology, its validity would highlight the importance of sample preparation in XRD data.

Transmission electron microscopy

To provide a better qualitative sense of the degree of clay exfoliation and dispersion engendered by the two melt-blending approaches, we present TEM images of the six samples in Figure 2. Here, it is immediately apparent that the SSE-scCO$_2$ and TSE processes induce manifestly different degrees of clay exfoliation and dispersion. At the 1 wt % loading, the clay tactoids in the TSE sample are smaller and more numerous, the largest of which have thickness of 25–75 nm and lateral dimension of 400–600 nm. Individual clay platelets are also apparent in this sample. By contrast, the 1 wt % scCO$_2$ sample contains larger clay agglomerates. The characteristic example captured in Figure 2(a)

TABLE I
Clay Basal Spacing Inferred from XRD Scans (Fig. 1) for Dry C15A Clay and Each Nanocomposite Sample

	C15A	1 wt % scCO$_2$	3 wt % scCO$_2$	5 wt % scCO$_2$	1 wt % TSE	3 wt % TSE	5 wt % TSE
Peak location (2θ)	2.71°	2.725°	2.72°	2.825°	2.715°	2.735°	2.69°
d_{001} spacing (Å)	32.6	32.4	32.5	31.2	32.5	32.3	32.8

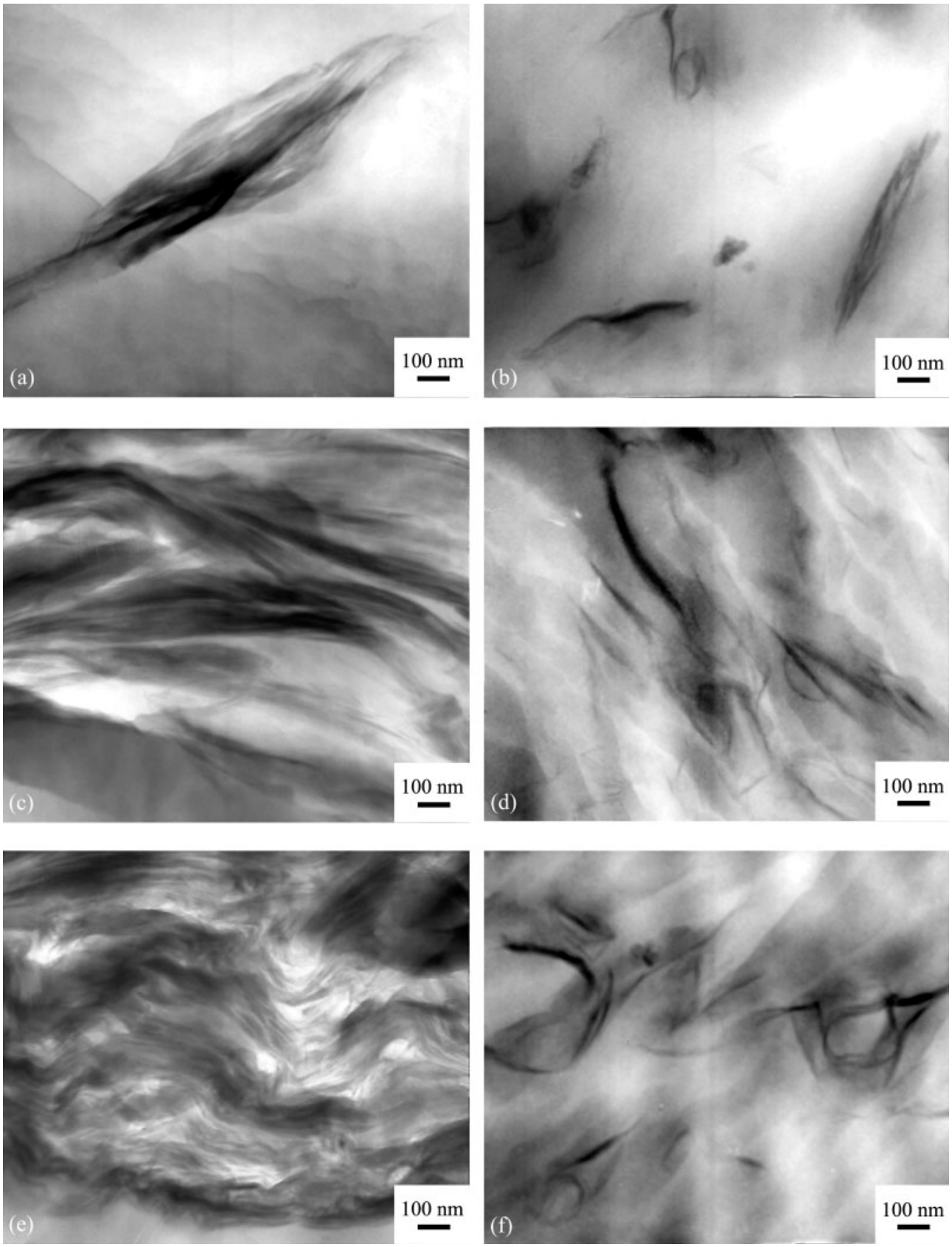

Figure 2 TEM images of (a) 1 wt % *sc*CO_2, (b) 1 wt % TSE, (c) 3 wt % *sc*CO_2, (d) 3 wt % TSE, (e) 5 wt % *sc*CO_2 nanocomposites and (f) 5 wt % TSE at ×60,000 magnification.

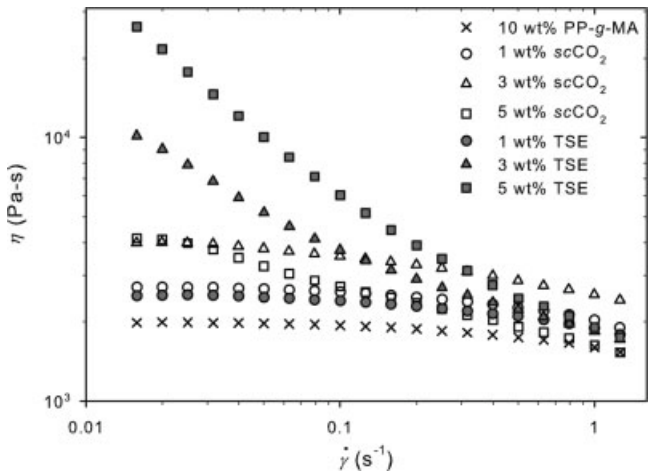

Figure 3 Viscosity versus shear rate for steady shear rate sweeps of 1, 3, and 5 wt % $scCO_2$ and TSE nanocomposites at 180°C.

is ≈ 300 nm thick and 1.3 μm long. However, in both cases, the 1 wt % samples are sparsely populated by clay domains and likely below the mechanical percolation threshold. Consequently, we might anticipate minimal differences in subsequent rheological tests.

At the 3 and 5 wt % clay loadings, the differences in the ability of the two processes to exfoliate and disperse clay leads to more significant differences in microstructure. The clay tactoids for the TSE materials in Figure 2(d, f) remain of similar scale to those observed for the 1 wt % clay loading in Figure 2(b), although the density of the tactoids must of necessity increase. On the other hand, the SSE-$scCO_2$ processed samples continue to contain agglomerated clay domains. Importantly, while the XRD results exhibited negligible differences in basal spacing for the six samples, TEM images suggest that the high shear of the twin-screw extruder has a much stronger influence in exfoliating and dispersing clay.

Rheology

The rheological response of filled polymers has previously been shown to be quite sensitive to particle loading, size, and dispersion.[17,29–32] PCNs have demonstrated a similar responsiveness to differences in clay exfoliation and dispersion, rendering rheology an effective indirect probe of microstructure.[6,19–21,24,25,33–35] In Figure 3, we report steady shear rate sweep data for the six nanocomposites as well as the 10 wt % PP-*g*-MA/90 wt % PP control sample. We first note that the zero-shear viscosity increases with clay loading for all samples, as expected, and all but the 3 and 5 wt % TSE samples exhibit the low shear rate plateau common to polymeric materials. For the 1 wt % clay samples, the shear rate responses are almost identical despite the differences in morphology observed in TEM, suggesting that neither material is percolated. However, the morphological differences observed in TEM translate to markedly different low shear rate response at the 3 and 5 wt % loadings. The 3 and 5 wt % TSE samples show the divergent viscosity behavior characteristic of mechanical percolation in PCNs and indicative of a nonzero yield stress.[2,20,24,25] By contrast, the similar $scCO_2$ materials show, at most, a modest divergence in viscosity at low shear rate. The finite yield stress can be determined by fitting the low shear rate data to Casson's equation, given as[25,36]:

$$\sigma_{xy}^{1/2} = \sigma_0^{1/2} + a\dot{\gamma}^{1/2}, \quad (1)$$

where σ_0 is the yield stress, and the parameter a is an arbitrary constant. The results of this analysis are presented in Figure 4, where the stronger dependence of yield stress on clay loading for the TSE nanocomposites is apparent. It has been hypothesized that the finite yield stress is caused by the formation of a mesoscale clay network.[18,24,35] When a deformation in excess of the yield stress is imposed, the clay network is ruptured, and the anisotropic clay domains align in the flow direction to a degree that depends upon the magnitude of the deformation. Thus, as the shear rate increases, clay domains become increasingly oriented in the flow direction and the shear viscosity decreases. Because the $scCO_2$ samples contain larger clay domains (agglomerated tactoids), the formation of a mesoscale network requires a higher clay loading than the better exfoliated and dispersed TSE samples. As a result, the zero-shear viscosity of the $scCO_2$ samples increases with clay loading like any filled polymeric material, but the inferred yield stress remains low. It should be noted, however, that the 5 wt % $scCO_2$ sample begins to shear thin at a lower shear rate than its

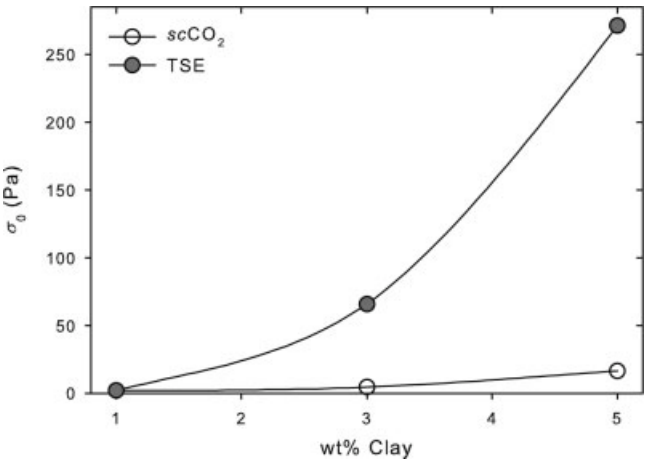

Figure 4 Apparent yield stress inferred from Casson's equation versus clay loading for 1, 3, and 5 wt % $scCO_2$ and TSE nanocomposites.

3 wt % counterpart, perhaps indicating that the clay loading is sufficiently high for a mesoscale clay network to form even in this poorly exfoliated material.

A change in the terminal response to SAOS is another signature of the transition from liquid-like (i.e., $G' \propto \omega$ and $G'' \propto \omega$) to solid-like (i.e., G', $G'' \alpha \omega^0$) behavior in filled polymeric materials, including carbon black,[29,31] calcium carbonate,[32] talc,[17] and clay filled systems.[18–23] In the case of clay, the solid-like terminal response has been attributed to the formation of a mesoscale clay network. Figure 5 shows TTS master curves (data shifted to 180°C) of the storage modulus, loss tangent (tan $\delta = G''/G'$), and complex viscosity ($|\eta^*|$) as a function of shifted frequency for blended nanocomposites and the 10 wt % PP-*g*-MA/PP sample. Because it is not a strong function of clay loading or processing method, data for the loss modulus are not reported. A distinct plateau in the storage modulus at low frequencies is observed for the 3 and 5 wt % samples, whereas only the 5 wt % *sc*CO_2 sample shows any significant deviation from classic liquid-like behavior. The loss tangent data are particularly illustrative of the transition to a more solid-like response. Values of the loss tangent greater than unity are characteristic of a liquid-like material (since the viscous response is much larger than the elastic), while values less than unity denote a more solid-like material. In Figure 5(b), the 3 and 5 wt % TSE and 5 wt % *sc*CO_2 samples have an inflection point in the loss tangent in the low frequency regime, leading to a decrease in loss tangent (or an increase in solid-like behavior) with decreasing frequency. Such behavior contrasts the other samples, whose loss tangent diverges to infinity (a liquid-like response) with decreasing frequency. Notably, however, the 5 wt % *sc*CO_2 material remains less solid-like than both the 3 and 5 wt % TSE samples. As suggested in the discussion of the steady shear rate sweep data, we believe that the clay loading for the poorly exfoliated and dispersed 5 wt % *sc*CO_2 sample is on the cusp of forming a solid-like, mesoscale clay network. Finally, the validity of the Cox-Merz rule may be assessed by comparing the data for steady shear viscosity in Figure 3 with those for complex viscosity in Figure 5(c). In general, Cox-Merz is obeyed for all but the 3 and 5 wt % TSE and 5 wt % *sc*CO_2 samples, suggesting that the failure of Cox-Merz is linked to the formation of a mesoscale clay network and yield behavior.

Several authors have reported that the strain at which the rheological response becomes nonlinear during oscillatory strain sweeps is sensitive to clay loading and morphology.[22,25,26] This critical strain (γ_c) has been observed to be inversely proportional to the volume fraction of clay (ϕ), as shown in eq. (2):

$$\gamma_c \propto \frac{1}{\phi}. \quad (2)$$

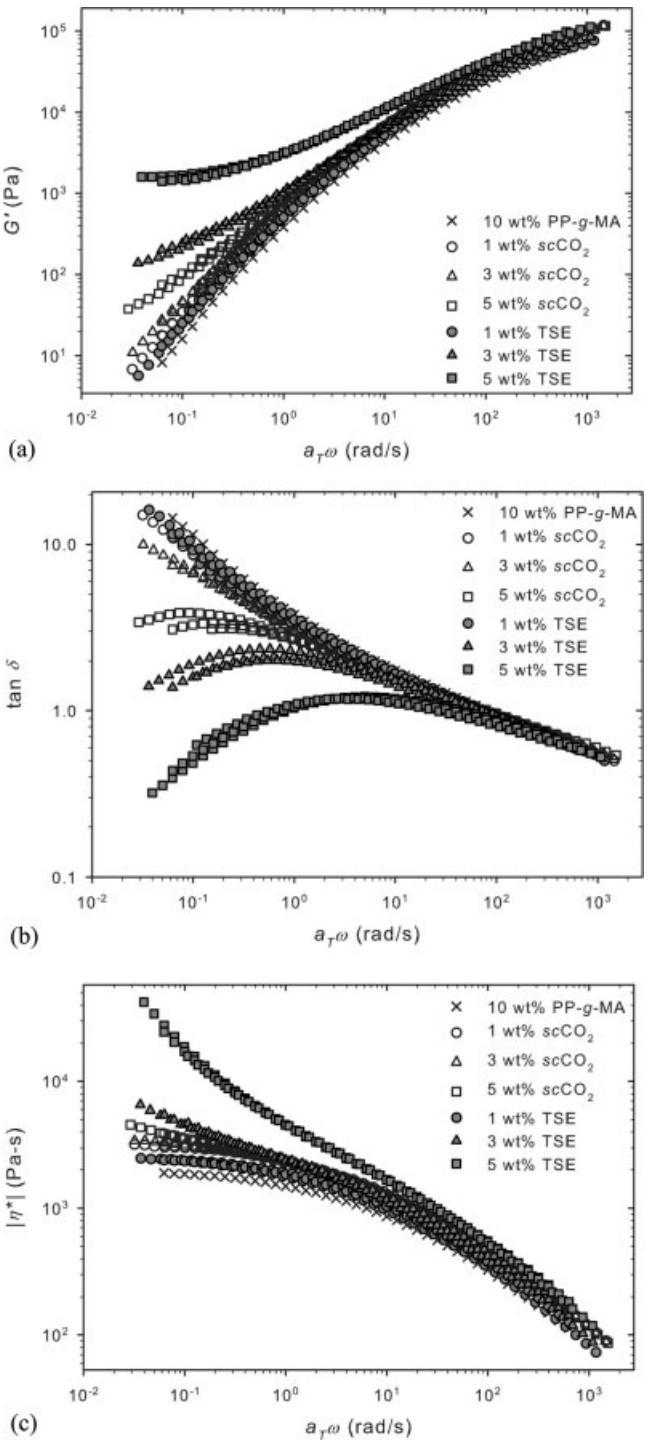

Figure 5 (a) Storage modulus, (b) loss tangent, and (c) complex viscosity versus frequency in oscillatory shear of 1, 3, and 5 wt % *sc*CO_2 and TSE nanocomposites and 10 wt % PP-*g*-MA/PP blended sample. Data were recorded at 150, 180, and 210°C and shifted to 180°C using time–temperature superposition. The strain amplitude was 0.01.

Figure 6 shows the results of oscillatory stress sweeps, where the data have been normalized by the complex viscosity at low strain to present all samples on the same figure and thereby better elucidate

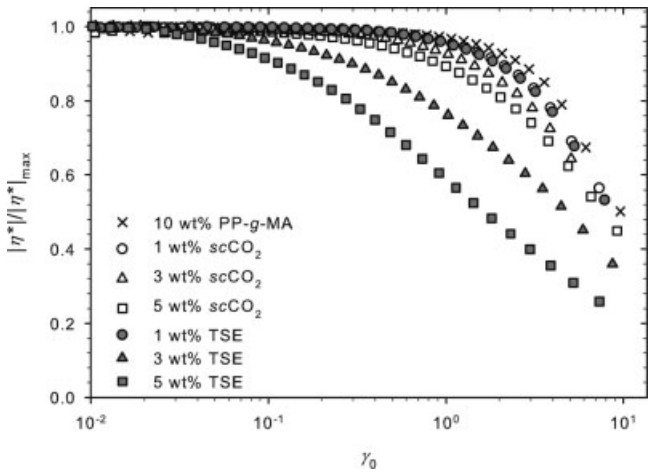

Figure 6 Normalized complex viscosity versus strain amplitude in oscillatory shear of 1, 3, and 5 wt % $sc$$CO_2$ and TSE nanocomposites and 10 wt % PP-*g*-MA/PP blended sample. Data were recorded at 180°C and a frequency of 1 rad/s.

differences in critical strain. Also, although the magnitude of the oscillatory stress was controlled during the experiment, the data are plotted versus strain amplitude. For a given blending method, it is evident that a higher clay loading does indeed lead to nonlinear behavior at lower strain values. The influence of clay loading is more pronounced for the TSE samples, which is again attributable to the more significant development of the solid-like, mesoscale clay network. The critical strain for each material was selected as the point at which the complex viscosity data deviated by 10% from the linear plateau value. These values are plotted versus inverse volume fraction in Figure 7. Although only three volume fractions are available for each blending method, the data adhere to the previously observed linear trend. At constant clay loading, the TSE samples have significantly lower critical strain values than the $sc$$CO_2$ counterparts. It has been suggested that lower critical strain results stem from the disruption of the mesoscale network by flow. Therefore, for a fixed clay loading, one may infer that a well-exfoliated and dispersed nanocomposite material will have a lower critical strain than a material with noninteracting, agglomerated tactoids domains. Thus, oscillatory strain data offer another convenient means of comparing different melt-blending processes, in this case demonstrating the efficacy of the TSE process relative to the SSE-$sc$$CO_2$ process.

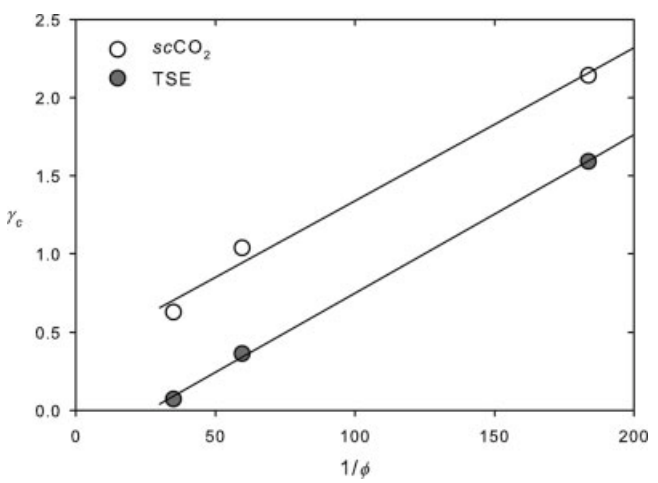

Figure 7 Critical strain versus inverse volume fraction of clay for 1, 3, and 5 wt % $sc$$CO_2$ and TSE nanocomposites.

Nanoindentation

Finally, nanoindentation experiments were performed on solid samples to assess the effect of processing, exfoliation, and dispersion on modulus. Figure 8 shows modulus data for the 3 and 5 wt % nanocomposites prepared using the two melt-blending processes along with the 10 wt % PP-*g*-MA/PP sample. Before proceeding, it is important to discuss how these mechanical measurements are best compared. Because of its lower molecular weight, PP-*g*-MA is known to have a plasticizing effect when blended with PP,[37] which can adversely affect impact performance.[38] At the same time, the inclusion of clay can improve impact performance, depending upon the degree of exfoliation and dispersion. Because of the dual influences of clay loading and PP-*g*-MA concentration, the 10 wt % PP-*g*-MA/PP control may only be compared with the 3 wt % samples, which have similar PP-*g*-MA concentrations.

This being the case, we first turn attention to the 10 wt % PP-*g*-MA/PP and 3 wt % samples. The better exfoliation and dispersion generated by the TSE process leads to the largest enhancement in modulus, although the $sc$$CO_2$ sample was also strengthened by the presence of clay. The influence of processing is more pronounced at the 5 wt % loading. While

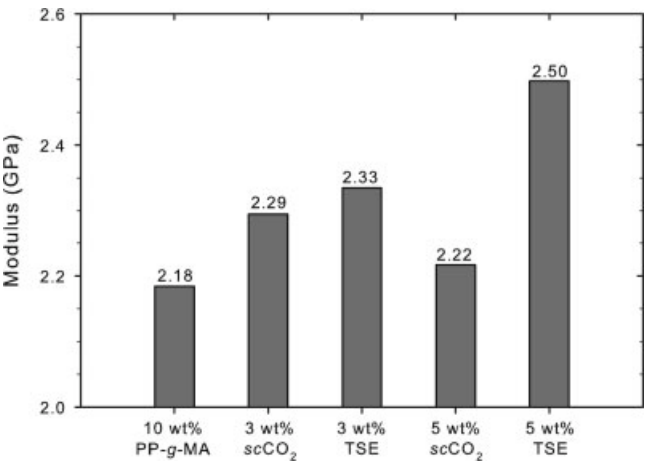

Figure 8 Modulus data recorded during nanoindentation of 3 and 5 wt % $sc$$CO_2$ and TSE nanocomposites and 10 wt % PP-*g*-MA/PP blended sample.

increasing the clay loading from 3 to 5 wt % in the $sc$$CO_2$ material leads to a decrease in the modulus, presumably due to the increased PP-*g*-MA concentration, the modulus of the 5 wt % TSE nanocomposite increases relative to that of the 3 wt % TSE material. Because the TEM and rheological experiments clearly indicate that the $sc$$CO_2$ nanocomposites contain large, poorly dispersed clay domains, the polymer blend appears to dominate the mechanical measurements in these materials. Alternatively, the better exfoliated clay domains in the TSE nanocomposites play a prominent role in strengthening the material despite increasing PP-*g*-MA concentration.

CONCLUSIONS

XRD, TEM, rheology, and nanoindentation experiments have been performed to contrast the ability of two melt-blending processes (SSE with an in-line $sc$$CO_2$ feed and twin-screw extrusion) to exfoliate and disperse MMT clay in compatibilized 1, 3, and 5 wt % polypropylene–clay nanocomposites. Although XRD failed to capture significant morphological differences at the basal spacing length scale, all other techniques suggest that the high shear of the TSE process is substantially more effective. TEM images reveal significantly smaller and more dispersed clay domains for the TSE samples, while steady shear and SAOS experiments show solid-like character at lower clay loading along with smaller critical strain values than the $sc$$CO_2$ counterparts. Nanoindentation further supports this conclusion, as the TSE nanocomposites exhibit larger moduli than $sc$$CO_2$ materials at the same clay and compatibilizer loading. The undesirable exfoliation and dispersion generated by the SSE-$sc$$CO_2$ process described here likely stems from two problems. First, the contact time between $sc$$CO_2$ and clay may be too short to allow significant diffusion into the clay intergallery. Second, thermodynamics limits the amount of CO_2 that polypropylene can solubilize, and that quantity may be insufficient to swell clay intergalleries during processing. As a result, we conclude that pretreating clay with $sc$$CO_2$ in pressurized vessels prior to extrusion may better promote clay exfoliation and dispersion. Moreover, the high shear and intense mixing of the TSE remains critical to the dispersion of clay in the polymer matrix.

The authors thank Dr. Robert Sammler of The Dow Chemical Company for the generous donation of the H700-12 polypropylene resin, Dr. Leigh Allen of Crompton Corp. for the Polybond® 3200 PP-*g*-MA compatibilizer, and Dr. Doug Hunter of Southern Clay Products for the Cloisite® 15A montmorillonite clay. We are also grateful to Prof. Donald Baird and graduate student Quang Nguyen in the Department of Chemical Engineering at the Virginia Polytechnic Institute for permitting the use of the SSE-$sc$$CO_2$ apparatus, Dr. Wei Zhang and Dr. Ronald Moffitt of the Advanced and Applied Polymer Processing Institute for the use of the Leistritz Micro 27 TSE, and Prof. Matthew Begley and graduate student John Gaskins in the Department of Mechanical and Aerospace Engineering at the University of Virginia for their assistance with the nanoindentation experiments.

References

1. Vaia, R. A.; Jandt, K. D.; Kramer, E. J.; Giannelis, E. P. Macromolecules 1995, 28, 8080.
2. Krishnamoorti, R.; Vaia, R. A.; Giannelis, E. P. Chem Mater 1996, 8, 1728.
3. Giannelis, E. P.; Krishnamoorti, R.; Manias, E. Adv Polym Sci 1999, 138, 107.
4. Ray, S. S.; Okamoto, M. Prog Polym Sci 2003, 28, 1539.
5. Marchant, D.; Jayaraman, K. Ind Eng Chem Res 2002, 41, 6402.
6. Lim, Y. T.; Park, O. O. Rheol Acta 2001, 40, 220.
7. Eckel, D. F.; Balogh, M. P.; Fasulo, P. D.; Rodgers, W. R. J Appl Polym Sci 2004, 93, 1110.
8. Zeng, C.; Lee, L. J. Macromolecules 2001, 34, 4098.
9. Lee, D. C.; Jang, L. W. J Appl Polym Sci 1996, 61, 1117.
10. Tomasko, D. L.; Han, X.; Liu, D.; Gao, W. Curr Opin Solid State Mater Sci 2003, 7, 407.
11. Garcia-Leiner, M.; Lesser, A. J. J Appl Polym Sci 2004, 93, 1501.
12. Dong, Z.; Liu, Z.; Zhang, J.; Han, B.; Sun, D.; Wang, Y.; Huang, Y. J Appl Polym Sci 2004, 94, 1194.
13. Manke, C. W.; Gulari, E.; Mielewski, D. F.; Lee, E. C. C. U.S. Pat. 6,469,073 B1 (2002).
14. Mielewski, D. F.; Lee, E. C. c.; Manke, C. W.; Gulari, E. U.S. Pat. 6,753,360 B2 (2002).
15. Garcia-Leiner, M. A. Ph.D. Dissertation, University of Massachusetts, Amherst, MA, 2004.
16. Li, G.; Li, H.; Wang, J.; Park, C. B. In the Annual Technical Conference – Society of Plastics Engineers, 2005, p 2332.
17. Suh, C. H.; White, J. L. J Non-Newton Fluid Mech 1996, 62, 175.
18. Krishnamoorti, R.; Yurekli, K. Curr Opin Colloid Interface Sci 2001, 6, 464.
19. Ren, J.; Casanueva, B. F.; Mitchell, C. A.; Krishnamoorti, R. Macromolecules 2003, 36, 4188.
20. Solomon, M. J.; Almusallam, A. S.; Seefeldt, K. F.; Somwangthanaroj, A.; Varadan, P. Macromolecules 2001, 34, 1864.
21. Galgali, G.; Ramesh, C.; Lele, A. Macromolecules 2001, 34, 852.
22. Li, J.; Zhou, C.; Wang, G.; Zhao, D. J Appl Polym Sci 2003, 89, 3609.
23. Gu, S.-y.; Ren, J.; Wang, Q.-f. J Appl Polym Sci 2004, 91, 2427.
24. Krishnamoorti, R.; Ren, J.; Silva, A. S. J Chem Phys 2001, 114, 4968.
25. Ren, J.; Krishnamoorti, R. Macromolecules 2003, 36, 4443.
26. Aubry, T.; Razafinimaro, T.; Mederic, P. J Rheol 2005, 49, 425.
27. Zhao, J.; Morgan, A. B.; Harris, J. D. Polymer 2005, 46, 8641.
28. Morgan, A. B.; Gilman, J. W. J Appl Polym Sci 2003, 87, 1329.
29. Lobe, V. M.; White, J. L. Polym Eng Sci 1979, 19, 617.
30. Khan, S. A.; Prud'homme, R. K. Rev Chem Eng 1987, 4, 205.
31. White, J. L.; Tanaka, H. J Appl Polym Sci 1981, 26, 579.
32. Suetsugu, Y.; White, J. L. J Appl Polym Sci 1983, 28, 1481.
33. Krishnamoorti, R.; Giannelis, E. P. Macromolecules 1997, 30, 4097.
34. Ren, J.; Silva, A. S.; Krishnamoorti, R. Macromolecules 2000, 33, 3739.
35. Lele, A.; Mackley, M.; Galgali, G.; Ramesh, C. J Rheol 2002, 46, 1091.
36. Casson, N. Rheology Disperse Systems; Pergamon: New York, 1959; p 84.
37. Zhang, Y.-Q.; Lee, J.-H.; Jang, H.-J.; Nah, C.-W. Compos, Part B: Eng 2004, 35, 133.
38. Hong, C. H.; Lee, Y. B.; Bae, J. W.; Jho, J. Y.; Nam, B. U.; Hwang, T. W. J Appl Polym Sci 2005, 98, 427.